iForest
Biogeosciences and Forestry

Research Article
doi: 10.3832/ifor4632-017
vol. 18, pp. 45-53

Mapping the vegetation and spatial dynamics of Sinharaja tropical rain forest incorporating NASA's GEDI spaceborne LiDAR data and multispectral satellite images

Dulan Jayasekara [(1)], **Tharanga Dhananjani** [(1-2)], **Vinuri Mendis** [(2-3)], **Harsha Jayawickrama** [(4)], **Tharanga Prasad** [(5)], **Maleesha M Gunarathna** [(6)], **Pethigelaye Gunarathna** [(5)], **Dharshani Mahaulpatha** [(1)]

This study integrates NASA's Global Ecosystem Dynamics Investigation (GEDI) spaceborne LiDAR data with multispectral satellite imagery to map the vegetation and assess spatial dynamics within the Sinharaja Forest Reserve (SFR), located in the southwestern Sri Lanka. Utilizing advanced remote sensing techniques, we delineated vegetation structure, vegetation density distribution, and canopy cover at high spatial resolutions. Eight distinct vegetation/land cover types were identified and an updated vegetation map was developed for SFR. The resulted map recorded an estimated overall accuracy of 90% (Kappa coefficient = 0.9) by the accuracy assessment. Comprehensive insights into forest composition and spatial dynamics were achieved with regard to canopy heights, plant area index and plant area volume density. Our results suggest that the integration of GEDI LiDAR and satellite imaging data offers a robust framework for characterizing tropical forest ecosystems, facilitating better understanding of their ecological processes, and informing conservation and management strategies.

Keywords: Forest Dynamics, Remote Sensing, Land Cover, Forest Ecology, Vegetation Density

Introduction

Tropical forests once covered 12 percent of Earth's terrestrial surface and have now been reduced to less than 5 percent (Corlett & Primack 2011, Hansen et al. 2013, Brandon 2014), indicating the level of exploitation and land cover change caused by the unprecedented human activities. Tropical rainforests are the most biodiverse and productive terrestrial ecosystems on Earth, providing numerous ecosystem services (Potapov et al. 2021). Warm temperatures, constant sunlight throughout the year, high precipitation, and high biodiversity lead to complex forest structures with multiple layers and a high species density. These aspects of tropical forests make vegetation mapping significantly more challenging, mainly when traditional methods are employed. The availability of accurate and detailed vegetation maps is an essential requirement in modern ecological studies (Gil et al. 2011, Jayasekara et al. 2021), providing critical information for a variety of applications ranging from land management, detecting forest cover changes, understanding biodiversity patterns, carbon cycling, vegetation protection, restoration programs, and conservation planning (Egbert et al. 2002, Dias et al. 2004, Xie et al. 2008, Xie et al. 2019, Li et al. 2020). In this context, with the constant development and evolution of remote sensing technologies, the availability of large Earth Observation (EO) datasets plays a vital role in vegetation mapping for both present and future applications. The significant improvements in spectral, temporal, and spatial resolutions of satellite imagery (*e.g.*, Landsat and Sentinel systems – Zurqani et al. 2018) and the availability of novel auxiliary data sets such as the NASA's Global Ecosystem Dynamics Investigation (GEDI) spaceborne Light Detection and Ranging (LiDAR) have opened new horizons in land cover (LC) mapping and investigating the structural dynamics of forests.

According to Tierney et al. (2017) vegetation maps are based on two essential elements: a classification of vegetation and a spatial attribution of that classification. Hence, the vegetation mapping groups together similar plant communities into a simplified form depicting their arrangement pattern with spatial reference (De Cáceres 2013). Landsat and Sentinel satellite missions provide two of the most prominent currently available free datasets of multispectral satellite imagery. The newest Landsat 8/9 and Sentinel 2 satellite images offer reasonably high spatial (up to 10 m) and spectral resolution, with multiple bands. Many land cover (LC) and vegetation mapping studies have utilized these multispectral satellite images for classification purposes in recent years. Xie et al. (2019) mentioned the importance of incorporating spatial-based variables into spectral features, which leads to improved clas-

(1) Department of Zoology, Faculty of Applied Sciences, University of Sri Jayewardenepura, Gangodawila (Sri Lanka); (2) Faculty of Graduate Studies, University of Sri Jayewardenepura, Gangodawila (Sri Lanka); (3) Faculty of Graduate Studies, University of Manitoba, Winnipeg, Manitoba, R3T 2N2 (Canada); (4) Faculty of Applied Sciences, Uva Wellassa University, Badulla 90000 (Sri Lanka); (5) Forest Department (Sri Lanka); (6) Faculty of Technology, University of Sri Jayewardenepura (Sri Lanka)

@ Dulan Jayasekara (dulan@sjp.ac.lk)

Received: Apr 26, 2024 - Accepted: Dec 05, 2024

Citation: Jayasekara D, Dhananjani T, Mendis V, Jayawickrama H, Prasad T, Gunarathna MM, Gunarathna P, Mahaulpatha D (2025). Mapping the vegetation and spatial dynamics of Sinharaja tropical rain forest incorporating NASA's GEDI spaceborne LiDAR data and multispectral satellite images. iForest 18: 45-53. – doi: 10.3832/ifor4632-017 [online 2025-04-01]

Communicated by: Marco Borghetti

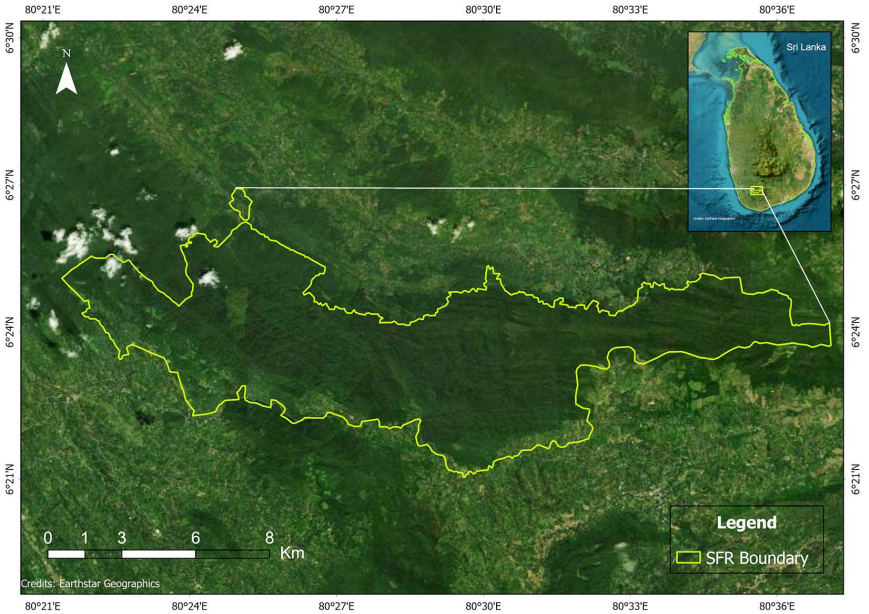

Fig. 1 - Map of Sinharaja Forest Reserve (SFR), SW Sri Lanka.

sification accuracy, as reported by Han et al. (2012) and Li et al. (2018). While spectral indices, such as Normalized Difference Vegetation Index (NDVI), are extensively used for forest classifications, the usage of auxiliary spatial data is uncommon. According to Xie et al. (2019), the use of forest stand structure features supports the separation of different forest types based on the tree species composition, canopy height, crown size and shape, and tree density. The difficulties in obtaining such data over large areas, based on air LiDAR, limit the number of studies that have incorporated these two aspects into forest classification. However, with the availability of NASA's GEDI data from spaceborne LiDAR sensors, which are explicitly designed to measure Earth's surface structure, including detailed information about the 3D canopy structure of terrestrial vegetation, there is the opportunity to utilize this data for forest classification. GEDI data generated by the sensor onboard the International Space Station (ISS) are available from March 2019, allowing the derivation of vertically resolved information related to canopy height, density, and layering through full waveform sampling (Hancock et al. 2019, Marselis et al. 2019, Schneider et al. 2020).

The tropical island of Sri Lanka had a considerable forest cover a few centuries ago, when many protected areas were not established yet. However, the drastic decline in forested areas of the island, which occurred in the last two centuries, has resulted in the current forest cover being less than 22% (Dittus 2017). The highest level of forest exploitation has occurred in the wet zone of the island, primarily due to increased anthropogenic activities and human settlement. Less than 2.1% of the original wet zone lowland forests still remain, and they occur as fragmented, degraded, and isolated patches (Kathriarachchi 2012). In this context, we focused this research on the Sinharaja Forest Reserve (SFR), which can be considered as Sri Lanka's largest, relatively undisturbed rainforest (De Zoysa & Raheem 1990, Gunatilleke et al. 2008). Although the first published mapping effort of the Sinharaja forest dates back to the comprehensive work by Baker (1937), only a handful of detailed vegetation maps are available for the area. Updated maps with detailed vegetation and LC details at high resolution are scarce. There is one study that has focused on mapping the carbon stock of SFR based on Landsat image analysis (Nissanka & Pathinayake 2009). Work by Madurapperuma & Kuruppuarachchi (2014) and Samarasinghe et al. (2022) have attempted to detect the LC changes of Sinharaja based on Landsat images focusing on spectral information. Additionally, Lockwood (2019) has conducted a classification attempt based on Planet Dove imagery. Wijesinghe & De Brooke (2005) categorized the primary and secondary vegetation as unlogged and selectively logged habitats. However, a map to represent the two habitat types is not available. When spatial dynamics of wet zone forests are considered, several plot-based studies have been conducted in the past (Ariyasena et al. 2017, Chandrasekara et al. 2005, Punchi-Manage et al. 2013). However, a remote sensing approach covering the whole SFR is not available. This research gap necessitates the requirement of an updated vegetation map. Our study was conducted with the objectives of developing a detailed vegetation map for SFR and utilizing modern remote sensing techniques to investigate the spatial dynamics of SFR vegetation structure.

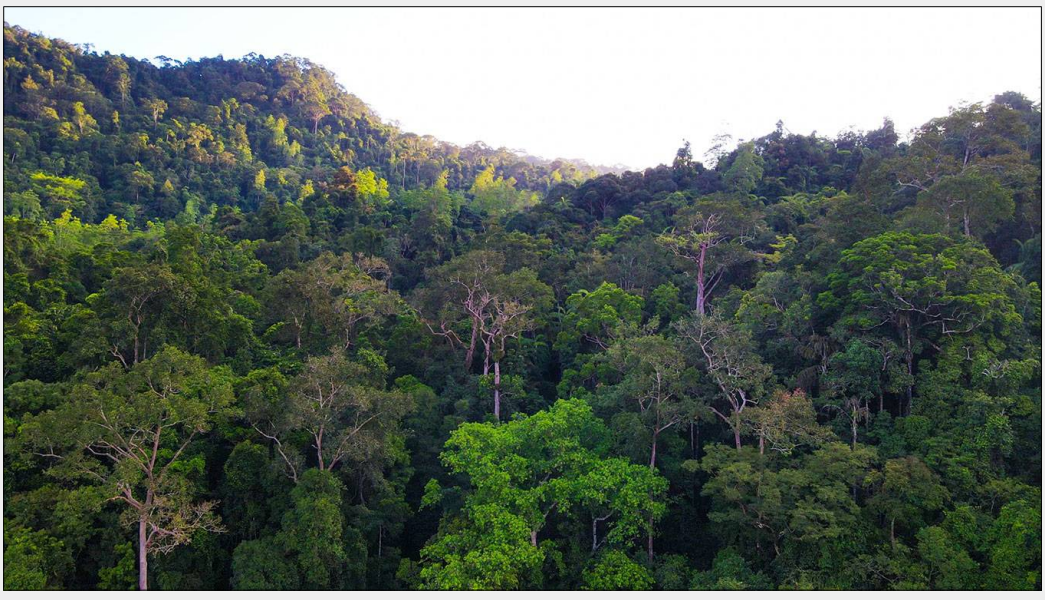

Fig. 2 - An aerial photograph of SFR partially showing the vertical profile and canopy strata.

Materials and methods

Study area

The study was conducted in Sinharaja Forest Reserve (SFR – Fig. 1) which is also a UNESCO World Heritage site (Gunatilleke et al. 2008). Sinharaja is a tropical dipterocarp rainforest that lies in the Southwest low and mid-country wet zone of Sri Lanka, between latitudes 6° 21′ - 6° 26′ N and longitudes 80° 21′ - 80° 34′ E. It covers an area of 11,187 ha and it is known to be the Sri Lanka's largest, relatively undisturbed rainforest (De Zoysa & Raheem 1990). This area is considered to harbor a relict of the Deccan-Gondwana biota and is recognized as the only aseasonal ever-wet region in South Asia (Ashton & Gunatilleke 1987, Gunatilleke et al. 2005). The steep hills and valleys of Rakwana Mountains, with nine peaks ranging from 575 to 1170 m, lie within the forest, creating complex topographies and elevation gradients. The mean annual rainfall at Sinharaja varies between 3600-5000 mm, and dry spells are rare (Bambaradeniya et al. 2006). Between 1971 and 1977, selective logging for plywood production was conducted in the western parts of Sinharaja. In 1978, an area of 8500 ha was declared an International Man and Biosphere (IMAB) Reserve and placed under the protection of the Forest Department. An additional 2687 ha of sub-montane forest located on the Eastern side was also included in the Sinharaja Reserve, expanding the total area to 11,187 ha. The forest vegetation consists mainly of primary and secondary tropical lowland wet evergreen rainforests, with areas of sub-montane forests (also known as lower montane forests – Gunatilleke et al. 2008) and grassland habitats at higher altitudes. Approximately 340 woody plant species, representing 71 families, have been recorded in Sinharaja, which accounts for approximately 35% of the woody plant species recorded in Sri Lanka. More than 60% of the woody plants recorded from Sinharaja are endemic to the island (Gunatilleke et al. 2008). In some plant families, such as Dipterocarpaceae, which dominate the forest canopy, endemism is more than 90%. The herbaceous plant community is equally rich. A diverse community of lower plants, including ferns, fungi, and bryophytes, is also found in Sinharaja (Bambaradeniya et al. 2006). Forest strata consist of ground layer, understory, sub-canopy, canopy, and emergent layer (Bambaradeniya et al. 2006 – Fig. 2).

Data acquisition and vegetation categorization

Landsat 8 and Sentinel 2 data

To obtain spatial and spectral information on vegetation types and land cover, we acquired multi-spectral images from Landsat 8 (launched in February 2013), Sentinel 2A (launched in June 2015), and Sentinel 2B (launched in March 2017) satellites from the United States Geological Survey online database (http://glovis.usgs.gov/). Landsat 8 images were orthorectified and terrain-corrected in the T1 collection (OLI_TIRS sensor/path_141/row_56). We used bands 2, 3, 4, 5, 6, and 7 of Landsat 8, which were acquired on February 20, 2019. Two Sentinel scenes were required to cover the study area, and images from Sentinel 2A (RA076, T44NMN) and 2B (RA119, T44) were used, taken in January 2022 and November 2021, respectively. The bands considered were 2 to 11. These spectral bands were combined in ArcGIS™ Pro (ESRI, Redlands, USA) to create multiband raster datasets using the "Composite Bands" tool. Several band combinations were used to obtain rich vegetation information and discriminate between vegetation, water, and dry land (Mtibaa & Irie 2016). We generated raster layers of several spectral indices, as listed in Tab. 1. Additionally, GEDI-derived PAI, PAVD vegetation indices, and canopy height were included in the initial set of variables. Elevation data was obtained using a Digital Elevation Model (DEM).

Topographic data

Digital Elevation Model (DEM) for the study area was obtained from version 3 of Advanced Spaceborne Thermal Emission and Reflection Radiometer (ASTER) GDEM data available at the United States Geological Survey online database (https://earthexplorer.usgs.gov/). The ASTER GDEM version 3 data are available in GeoTIFF format at a spatial resolution of 1 arcsecond (approximately 30 meters horizontal posting at the equator). The relationship between canopy height and elevation was investigated using the DEM extracted for SFR.

Categorization of vegetation types based on PCA analysis

Raster maps were generated for elevation, NDVI, GNDVI, NDMI, BSI, NDWI, CHM95, PAI and PAVD. IDW interpolation method was utilized for the generation of raster maps based on point data from CHM95, PAI and PAVD. The values contained in these raster maps were extracted into 131 randomly generated points in Ar-

Tab. 1 - Summary of spectral indices, vegetation/environmental parameters, and standard methods used. "x" indicates whether each parameter was considered in the final analysis.

Parameter	Abbreviation	Method used	Usage
Normalized Difference Vegetation Index	NDVI	NDVI is calculated from the reflectance values of two bands of electromagnetic radiation: near-infrared (NIR) and red (Grebner et al. 2013, Pantazi et al. 2020). NDVI = (NIR - RED) / (NIR + RED)	x
Bare Soil Index	BSI	The short-wave infrared and the red spectral bands are used to quantify the soil mineral composition, while the blue and the near-infrared spectral bands are used to enhance the presence of vegetation (Sykas 2020). (B11 + B4) - (B8 + B2) / (B11 + B4) + (B8 + B2)	x
Normalized Difference Moisture Index	NDMI	Normalized Difference Moisture Index is sensitive to variations in water content in leaves and can be useful for monitoring drought conditions, assessing vegetation health, and studying hydrological processes (Pantazi et al. 2020). (NIR - SWIR) / (NIR + SWIR)	-
Normalized Difference Water Index	NDWI	Average by quadrates (ocular estimation)	-
Moisture Stress Index (MSI)	MSI	The values of this index range from 0 to more than 3, with the common range for green vegetation being 0.2 to 2 (Ma et al. 2019). B11 / B08	-
Plant Area Index	PAI	GEDI derived	x
Plant Area Volume Density	PAVD	GEDI derived	x
Canopy Height Model (at rh95)	CHM95	GEDI derived	x
Elevation	ele	GEDI derived + DEMs from Advanced Spaceborne Thermal Emission and Reflection Radiometer (ASTER) dataset	x

cMap. The covariate selection process was carried out in three steps: (i) removal of covariates with variance close to zero; (ii) removal by correlation; and (iii) removal by importance (Da Silveira et al. 2022). This ensured that statistically insignificant covariates, multicollinearity, and covariates without contextual relevance were removed before the analysis. Principal component analysis (PCA) was performed using R version 4.3.3 (R Core Team 2024) to create clusters of similar vegetation/LC based on the standardized dataset. After accounting for multicollinearity (>75%), the number of covariates considered for the final analysis was four, including elevation, CHM95, NDVI, BSI, and PAVD. The ground survey data and visual identification were aided to predict the vegetation/LC category of each point.

Supervised classification of satellite images to generate vegetation/LC map

We conducted supervised classification for both Landsat 8 and Sentinel 2 images. However, the Sentinel 2 classification was retained, which resulted in higher accuracy. The spectral bands 2 to 11 were combined in ArcGIS Pro (Esri, Redlands, USA) to create a multiband raster dataset using the "Composite Bands" tool. Training samples were provided based on both ground survey data and visual observations. The generated raster maps of vegetation indices and forest vertical structure were also used to provide training samples. The training sample data set was supplemented with Arc GIS base map imagery data (Esri, Digital Globe) when clarifications of vegetation cover were required for inaccessible terrain and locations outside the survey areas. Major vegetation types identified from PCA were considered when providing training samples; High Forest (HF), Low Forest (LF), Sub-montane Forest (SMF), Home Gardens (HG). In addition to the main four categories observed from PCA, we included four other categories that were confirmed through ground surveys, albeit with very limited area coverage. Those included Grassland/Shrubland (GS), Other Vegetation (OV) (including cropland, plantation, and degraded forest), Marsh/Swamp (MS), and Waterbody/River (WR). Therefore, a total of eight classes were considered. Due to the close resemblance between HF and LF, we describe HF as mature forests with tall trees, typically part of primary or climax forest ecosystems, characterized by a rich and complex canopy. These are often associated with older, structurally diverse forests that have achieved a stable ecological state. LF can be described as areas with shorter trees and a less developed canopy structure. These may be secondary forests, degraded forests recovering from disturbances such as logging, or forests that grow in areas with less fertile soil or more challenging climatic conditions. Thus, HF and LF will be treated as separate habitat entities henceforth. Supervised image classification was conducted based on the maximum likelihood classification (MLC) algorithm. Removal of random noise was conducted through post-classification processing, which involved majority filtering, boundary cleaning, region grouping, setting null, and nibbling.

Reference data, ground truthing, and accuracy assessment

For classifier training and validation of the satellite-image-based classification, we used ground truth data acquired during field surveys conducted between January 2019 and May 2022. The field surveys covered diverse forest types of SFR, strategically selected to encompass varying entry points to the forest and also at different altitude levels following a stratified method. The ground truth data collection involved a set of randomly generated sampling points within each major forest type, totaling 132 survey points. The forest type at each sampling point, along with the average canopy height, was recorded. A minimum of three height measurements were obtained using a Prime 1700 Laser Range Finder® (Bushnell, USA) within a 20 m radius from the sampling point. The points that could not be reached or assessed *via* ground-based surveys were investigated using the visual inspection method. We visually inspected multitemporal imagery in Google Earth® Pro and ArcGIS™ base maps to identify the types of vegetation and land use. The assistance of forest rangers was obtained for the validation in instances where visual inspection was inconclusive.

An accuracy assessment was conducted to compare the predicted results (classification results) with ground reference data collected from both field observations and high-resolution base map imagery. Accuracy was validated using field observations and base-map imagery. An error matrix was prepared to evaluate classification accuracy, calculating both the overall and class-specific accuracies. Additionally, we computed the Kappa coefficient (κ) in ArcGIS Pro to assess the statistical reliability of the classifications relative to random chance. The Kappa coefficient (κ) was calculated using the equation (eqn. 1):

$$\kappa = \frac{p_O - p_e}{1 - p_e} \quad (1)$$

where p_o represents the observed accuracy (the proportion of correctly classified samples), and p_e represents the expected accuracy, which is the probability of random agreement among classifications. p_e was calculated by summing the products of row and column totals for each class in the error matrix, divided by the square of the total number of samples (eqn. 2):

$$p_e = \frac{\sum_{i-1}^{k} \left(n_{i+} \cdot n_{+i} \right)}{N^2} \quad (2)$$

where n_{i+} and n_{+i} are the row and column totals for class *i*, and *N* is the total number of samples. The kappa coefficient ranges from -1 to 1, where values close to 1 indicate a strong agreement between predicted and reference classifications.

Data acquisition and analysis of the spatial dynamics of forest structure

GEDI data

The GEDI spaceborne LiDAR system on board the International Space Station has near-global coverage between 51.6° and -51.6° latitude. The lasers on board produce four beams, resulting in eight-track ground transects. Geolocated waveforms are generated based on the laser energy return, which is tracked as a function of time. Several higher-level GEDI products are available following the processing of these waveforms. We utilized GEDI-derived Level 2A (L2A) and Level 2B (L2B) data to obtain measurements of forest canopy height, vertical canopy structure, and surface elevation. GEDI L2A data contain the coordinates, elevation, and relative height metrics (rh 0-100) extracted from return waveforms of the various reflecting surfaces located within each laser footprint. GEDI also possesses an accuracy of less than 1 m bias in canopy height measurement (Wang et al. 2022). The GEDI L2B standard data product adds vertical profile metrics: canopy cover (CCGEDI), plant area index (PAI), estimated vertical canopy directional gap probability for the selected L2A algorithm (PGP_THT), foliage height diversity index (FHD), and plant area volume density (PAVD) for each laser footprint located on the land surface. A bounding box extending the area of SFR was used to select all the GEDI beams within the study area. We retrieved GEDI laser shots available from 2019 to October 2022 (Fig. S1 in Supplementary material) from NASA LP DAAC (Land Processes Distributed Active Archive Center – https://lpdaac.usgs.gov/product_search/). The downloaded GEDI granules in HDF5 format were processed in R version 4.3.3 (R Core Team 2024) using the rGEDI package (Silva et al. 2023) to subset and generate shape files usable in ArcGIS Pro. We filtered only the high-quality GEDI shots for the study area using the attribute Quality Flag (QF=1) and Sensitivity (SF<0.9). We disregarded all other shots to meet the quality criteria based on energy, sensitivity, amplitude, and real-time surface tracking (Dubayah et al. 2020, Dorado-Roda et al. 2021). For canopy height metrics, we used the rh95 values of the L2A product, which is defined as the elevation difference between ground elevation and the elevation where the accumulated waveform energy is 95% of the total (Potapov et al. 2021, Wang et al. 2022). Using L2B granules, the PAI was obtained as cumulative values to represent the prominent forest strata at heights of 5-15 m (lower canopy, including the understory), 15-30 m (sub canopy), and >30 m (canopy) levels (Gunatilleke & Gu-

natilleke 1985) and as an overall cumulative value from 0-45 m for mapping. PAVD was also obtained for the same height categories.

Results

Vegetation categorization and mapping

The principal component analysis revealed four major vegetation types; High Forest (HF), Low Forest (LF), Sub-montane Forest (SMF), Home Gardens (HG), and a considerable clustering was observed between the vegetation classes (Fig. 3). Based on the Eigen correlation matrix (Tab. 2), the first three principal components accounted for 84% of the total variance. BCI and NDVI contributed significantly to PC1, which clustered the HG with other vegetation types. Significant components in PC2 were CHM and PAVD, where HF and LF were separated. Canopy height can be used as a demarcating factor for HF and LF, and we propose considering lowland areas with a 15-25 m canopy as LF and those with a canopy height > 25 m as HF. Elevation was significantly contributing to PC3 influencing the clustering of SMF (Tab. 3).

In addition to the four major vegetation/LC classes, SFR comprises four other minor vegetation/LC classes, which were identified during our ground surveys as well as in the image classification (Fig. 4). These include Marsh/Swamp (MS), Grassland/Shrublands (GS), Other vegetation (OV) and Waterbodies (river/stream, WR). The accuracy of the classification is indicated by an overall Kappa coefficient value of 0.9 (Tab. 4). Except for the MS category, all other classes recorded accuracy values higher than 0.7. HF was the most dominant vegetation type, covering 38% of the area and extending over 4355.8 ha. It was followed by LF, covering 29% of the study area (Tab. 5).

Vegetation and spatial dynamics

A total of 7566 GEDI footprints were present within the study area before filtering (Fig. S1 in Supplementary material). It was reduced to 1778 and 1848, respectively, for GEDI L2A and GEDI L2B, following the filtering for quality and degraded footprints. When canopy height values were plotted against elevation, the canopy height reached a peak around 500 m a.s.l. and gradually decreased at high altitudes in the Morningside region of Eastern Sinharaja (Fig. 5). A maximum NDVI of 0.86 was present within the forest vegetation, and the NDVI greatly fluctuates at different parts of the forest landscape (average: 0.44 ± 0.01 – Fig. S2b in Supplementary material). Overall, the rich vegetation density of SFR is visible from the NDVI map. PAI of a single canopy stratum ranged between 0 to 9.79 (average: 1.96 ± 0.02), and a similar pattern was observed for PAVD, which ranged from 0 to 1.22 (0.16 ± 0.001 – Fig. S2c, Fig. S2d). When cumulative PAI values at different canopy strata were plotted

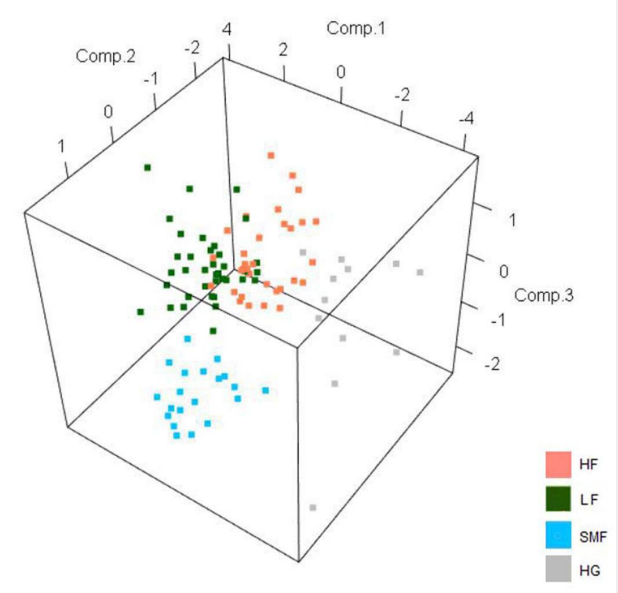

Fig. 3 - PCA 3D plot along the three principal component axes, displaying the main vegetation categories derived from the PCA analysis.

Tab. 2 - Eigen analysis of the correlation matrix.

Variable	PC1	PC2	PC3	PC4	PC5
Eigenvalue	1.922	1.387	0.936	0.442	0.314
Proportion	0.384	0.277	0.187	0.088	0.063
Cumulative	0.384	0.662	0.849	0.937	1.000

Tab. 3 - Eigenvector matrix of principal components with variable scores.

Variable	PC1	PC2	PC3	PC4	PC5
Elevation	-0.285	0.209	-0.896	-0.269	-0.020
CHM (rh95)	0.385	0.600	0.192	-0.551	-0.389
BSI	0.559	-0.367	-0.139	-0.459	0.568
NDVI	-0.532	0.380	0.329	-0.282	0.621
PAVD	0.419	0.563	-0.184	0.578	0.373

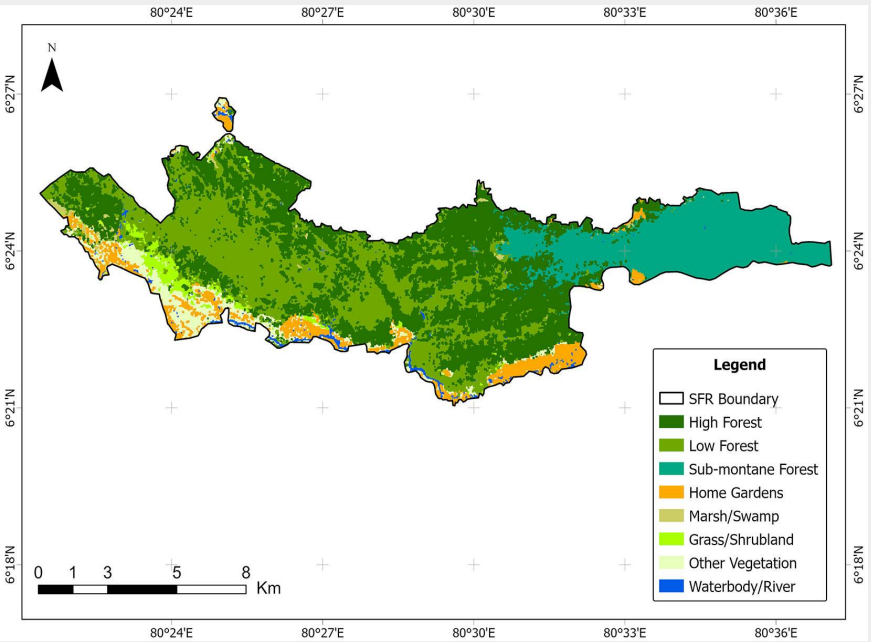

Fig. 4 - Vegetation and Land cover map of Sinharaja Forest Reserve. The map may not exclusively represent the legislated boundary.

Tab. 4 - Kappa coefficient accuracy matrix for classified SFR map. Overall kappa was 0.9.

Vegetation/Land cover type	Home Gardens/ Croplands	Marsh/ Swamp	Low Dense Forest	Grassland/ Shrubland	Dense Forest	Other vegetation	Water-bodies	Sub-montane Forest	Total	User Accuracy
Home Gardens/Croplands	10.0	0.0	0.0	0.0	0.0	0.0	0.0	0.0	10.0	1.0
Marsh/Swamp	0.0	7.0	2.0	1.0	0.0	0.0	0.0	0.0	10.0	0.7
Low Forest	0.0	0.0	27.0	0.0	0.0	0.0	0.0	0.0	27.0	1.0
Grassland/Shrubland	0.0	0.0	2.0	7.0	0.0	1.0	0.0	0.0	10.0	0.7
High Forest	0.0	0.0	3.0	0.0	32.0	0.0	0.0	2.0	37.0	0.9
Forest Plantations	0.0	0.0	1.0	0.0	1.0	8.0	0.0	0.0	10.0	0.8
Waterbody/River	2.0	0.0	0.0	0.0	0.0	0.0	8.0	0.0	10.0	0.8
Sub-montane Forest	0.0	0.0	0.0	0.0	0.0	0.0	0.0	18.0	18.0	1.0
Total	12.0	6.0	35.0	8.0	34.0	9.0	8.0	20.0	132.0	-
Production Accuracy	0.8	1.0	0.8	0.9	0.9	0.9	1.0	0.9	0.0	0.9

Tab. 5 - Percentage coverage and actual area of different vegetation/land cover types.

Vegetation/Land cover type	Percentage land cover (%)	Area (ha)	Area (km^2)
High Forest (HF)	38	4355.8	43.6
Low Forest (LF)	29	3307.6	33.1
Sub-montane Forest (SMF)	18	2059.9	20.6
Other Vegetation (OV)	5	536.8	5.4
Home Gardens (HG)	6	732.4	7.32
Grassland/Shrubland (GS)	2	233.1	2.3
Waterbody/River (WR)	1	125.6	1.3
Marsh/Swamp (MS)	1	87.7	0.9
Total	-	11439	114.4

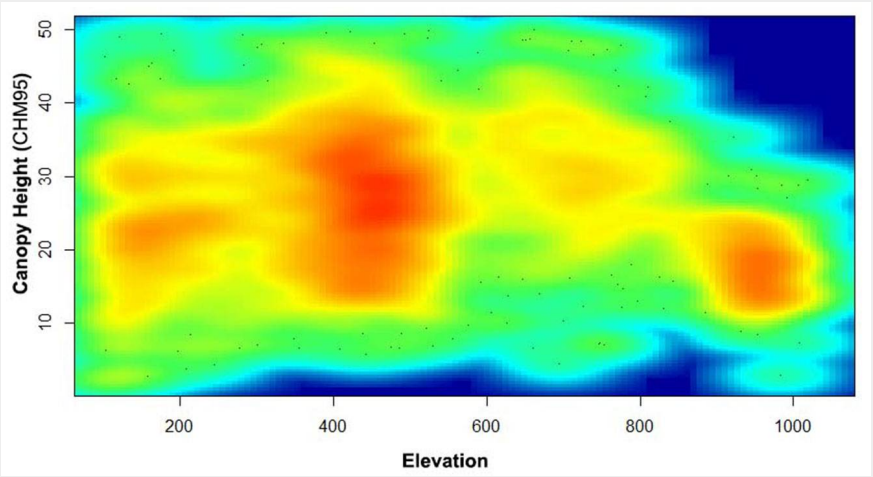

Fig. 5 - Variation of GEDI-derived canopy height (CHM, rh95) with elevation. Heat map range: high point density - red, low point density - blue.

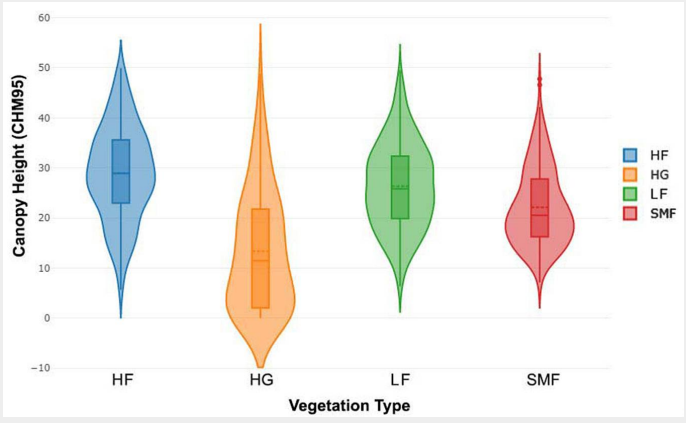

Fig. 6 - Canopy height violin plot for the major vegetation types in SFR.

against the main four vegetation classes (Fig. S3 in Supplementary material), the low overall PAI at all three canopy layers was visible for HG. The variation was limited among the other three major vegetation types. However, the higher PAI at high and mid-canopy layers of HF was visible from the violin plot, while LF and SMF had a relatively lower distribution of PAI values, respectively. As depicted in Fig. S4 (Supplementary material), the variability of PAVD at different canopy strata and the influence of total canopy height on PAVD are clearly visible (Fig. S4a, b, c, d, and e).

Of the main four vegetation/LC categories, the canopy height was lowest at HG (average: 13.35 ± 1.15 m). The second-lowest canopy height among the top four vegetation types was SMF (average: 22.12 ± 0.42 m). The highest canopy heights were observed in HF (average: 29.01 ± 0.39 m) and LF (average: 25.34 ± 0.37 m – Fig. S2e, Fig. 6), which reached maximum heights of > 60 m occasionally.

Discussion

Our study focused on delineating the vegetation and land cover patterns within SFR. Eight distinct categories have been identified, highlighting the complexity of vegetation and land cover patterns in the area. However, four prominent categories HF, LF, SMF, and HG dominate the landscape, covering the majority of SFR. Both HF and LF areas fall under the tropical lowland wet evergreen rainforest ecosystem described by Gunatilleke et al. (2008), with distinctions arising from past selective logging and naturally low vegetation density, including canopy cover. This prompted us to treat HF and LF as separate habitat entities in our analysis. We refrained from using terms like "Primary Forest" and "Secondary Forest" / "semi-logged forest" as they inadequately represented the current state of the forest, particularly given the substantial succession in semi-logged areas and variable vegetation density, especially in ridge forest areas. These two categories collectively constitute 67% of the forest reserve, representing areas of climax vegeta-

tion. HF areas primarily consist of remnants of climax tropical lowland wet evergreen rainforest, including selectively logged areas that have undergone succession. Notably, the sub-montane forest is confined to elevations ~900m a.s.l., in line with the description of Gunatilleke et al. (2008), covering an area of 18% predominantly in the eastern part of the reserve known as the "Morningside". Despite being designated as a Man and Biosphere Reserve, human settlements and cultivated landscapes occupy less than 15% of the total area, with the remaining area comprising small clusters of grasslands and shrublands, marshes and swamps, and water bodies, such as rivers and streams. This habitat diversity underscores the complexity of the vegetation and land cover mosaic characteristics of this World Heritage Forest landscape.

The elevation gradient of the forest reserve is vividly portrayed in the elevation map (Fig. S2a in Supplementary material) with the complex terrain that encompasses the region. Elevation proves to be a significant factor in shaping vegetation types in SFR. Our findings align with the work of Ediriweera et al. (2008) regarding the negative relationship between canopy height and elevation at higher altitudes. However, we found a positive trend between canopy height and elevation up to 500 m a.s.l., which was not reported in previous studies (Fig. 5).

A noteworthy observation is the highest Plant Area Index (PAI) of low canopy recorded in LF areas, likely due to ongoing succession fuelled by increased sunlight penetration through upper canopy openings. Consistent with previous studies, low PAI in sub-montane forests (SMF) at higher altitudes correlates with declines in leaf area index above 1000 m a.s.l., as noted by Madhumali et al. (2021). When plotted against canopy height, Plant Area Volume Density (PAVD) illustrated distinct variations among major vegetation classes, with HF exhibiting the densest vegetation structure, followed by LF, SMF, and GS.

Elevation exerts a pronounced influence on canopy height, reflecting climatic variability. Mid-elevation areas have the highest average canopy height, while elevations above 500 m experience decreased heights due to wind impacts, creating an intermediate vegetation structure between tropical lowland and montane forests, which we identify as sub-montane forests. However, ridge areas also exhibit relatively lower canopy heights, while valleys have the tallest trees, sometimes reaching >60 m. The average canopy height for lowland forests is 25-30 m, dropping to ~20 m in sub-montane forests. Areas of home gardens and croplands are characterized by lower canopy heights, ranging 0-15 m. PAI and PAVD also display a similar pattern, with the highest values in valley areas and lower values in ridges and higher elevations.

This study marks the first attempt to utilize GEDI data for assessing forest canopy height and structural dynamics in Sri Lanka. Wang et al. (2022) identified GEDI as a next-generation spaceborne LiDAR capable of revolutionizing global measurements of vertical vegetation structure. While NASA GEDI data and satellite imagery from Landsat 8 and Sentinel-2 have greatly enhanced our ability to analyze forest canopy structure and classification, several limitations and uncertainties should be acknowledged. GEDI's data coverage is limited by its spatial sampling pattern, which is determined by the International Space Station's orbit and the instrument's footprint distribution. This creates gaps in GEDI coverage, particularly in regions outside the main orbital path, reducing the representativeness of the data across the entire study area. Additionally, GEDI's vertical resolution is sensitive to terrain variations, making it less accurate in areas with steep slopes, where ground elevation and vegetation height may be misinterpreted. Both Landsat 8 and Sentinel-2 provide high-resolution multispectral imagery suitable for vegetation classification; however, their spatial resolution limits the detection of fine-scale forest heterogeneity, potentially leading to classification errors in mixed-vegetation areas or small forest patches.

SFR is one of the most biodiverse rainforest ecosystems in the world, and is of significant national and international importance. Our study fills the void regarding an updated vegetation map for the area. The versatility of GEDI database facilitated further investigation into the spatial dynamics of forest structure, particularly vertical dynamics. While acknowledging the significant contributions of long-term forest plot-based research (Ariyasena et al. 2017, De Cáceres et al. 2018, Gunatilleke & Gunatilleke 1985), we emphasize the need for holistic spatial approaches that encompass larger areas, thereby providing a broader understanding of spatial forest dynamics. Spaceborne LiDAR, as well as aerial LiDAR, can be identified as novel remote sensing techniques with greater potential for such research endeavors. Furthermore, our findings underscore the significance of spatial and remote sensing approaches, such as spaceborne LiDAR and multispectral remote sensing, in comprehensively understanding complex tropical forest ecosystems. By highlighting the practical application of these techniques, our study advocates for their broader adoption in future research endeavors aimed at elucidating forest dynamics.

The findings of this study have important implications for the forest management and conservation of SFR. By providing a high-resolution, spatially detailed vegetation map and insights into the vertical forest structure, this study offers a comprehensive understanding of the spatial composition of SFR. The methods adopted in our work provide a reliable framework for detecting deforestation, forest degradation, and habitat fragmentation over time, enabling early intervention to mitigate these threats. Moreover, identifying areas with dense vegetation presents opportunities for targeted conservation strategies. These insights support adaptive, evidence-based forest management policies that enhance climate resilience, promote long-term monitoring, and strengthen the conservation of tropical rainforest ecosystems such as Sinharaja.

Conclusion

This study presents an updated vegetation/LC map generated for SFR with high precision, spatial accuracy, and spatial resolution. Eight distinct land cover types were identified utilizing modern remote sensing methods such as spaceborne LiDAR and multispectral satellite imagery. Based on the NASA's GEDI datasets, the spatial dynamics of SFR were investigated in detail for the first time, filling the current research gap. The obtained results can be effectively used for conservation and management purposes, serving as an essential foundation for future ecological research.

Author Contributions

D.J. and D.M. conceived and conceptualized the research; DJ designed the methodology; D.J., D.M., T.D., V.M., H.S., P.G., M.G., T.P. conducted field surveys; D.J. conducted the formal analysis; D.J. wrote the first draft and D.M., V.M. reviewed and edited the manuscript. All authors discussed the results, provided feedback on the manuscript, and approved the final draft.

Conflicts of Interest

The authors declare that they have no competing interests.

Acknowledgment

The authors would like to acknowledge the support received from the staff of SFR, including Mr. Waththegama. We would also like to express our gratitude to the University of Sri Jayewardenepura for the facilities granted and the financial support provided to conduct this research under the university grant ASP/01/RE/SCI/2018/31. Funding provided by the Rufford Small Grants program (no. 31593-1) is also acknowledged.

References

Ariyasena L, Ekanayake U, Gunatilleke N, Gunatilleke S, Punchi-Manage R (2017). Spatial Patterns of Trees in the Sinharaja Forest in Sri Lanka. Proceeding of the "15th Open University Research Sessions" (OURS 2017). The Open University of Sri Lanka, Nawala, Sri Lanka, pp. 505-508.

Ashton PS, Gunatilleke CVS (1987). New light on the plant geography of Ceylon. I. Historical plant geography. Journal of Biogeography 14: 249-285. - doi: 10.2307/2844895

Baker JR (1937). The Sinharaja rain-forest, Ceylon. The Geographical Journal 89 (6): 539-551. -

doi: 10.2307/1787913
Bambaradeniya CNB, Amarasinghe S, Ekanayake SP (2006). Guide to Sinharaja: a biodiversity hotspot of the world. IUCN Sri Lanka, Colombo, Sri Lanka, pp. 51.
Brandon K (2014). Ecosystem services from tropical forests: review of current science. Center for Global Development, Washington, DC, USA, pp. 1-82. - doi: 10.2139/ssrn.2622749
Chandrasekara CMCP, Weerasinghe HMSPM, Gunatilleke IAUN, Seneviratne G (2005). Spatial distribution of arbuscular mycorrhizas along an elevation and adaphic gradient in the forest dynamics plot at Sinharaja, Sri Lanka. Ceylon Journal of Science, Biological Sciences 34: 47-67. - doi: 10.5555/20063026259
Corlett RT, Primack RB (2011). Tropical rain forests: an ecological and biogeographical comparison. John Wiley and Sons. Sussex, UK, pp. 336. [online] URL: http://books.google.com/books?id=KTCVw_RDlLkC
Da Silveira VA, Veloso GV, De Paula HB, Dos Santos AR, Schaefer CEGR, Fernandes-Filho EI, Francelino MR (2022). Modeling and mapping of Inselberg habitats for environmental conservation in the Atlantic Forest and Caatinga domains, Brazil. Environmental Advances 8: 100209. - doi: 10.1016/j.envadv.2022.100209
De Cáceres M (2013). Vegetation classification. Oxford University Press, website. [online] URL: http://www.oxfordbibliographies.com/display/document/obo-9780199830060/obo-9780199830060-0115.xml
De Cáceres M, Franklin SB, Hunter JT, Landucci F, Dengler J, Roberts DW (2018). Global overview of plot-based vegetation classification approaches. Phytocoenologia 48 (2): 101-112. - doi: 10.1127/phyto/2018/0256
De Zoysa N, Raheem R (1990). Sinharaja, a rain forest in Sri Lanka. March for Conservation, Colombo, Sri Lanka, pp. 61.
Dias E, Elias RB, Nunes V (2004). Vegetation mapping and nature conservation: a case study in Terceira Island (Azores). Biodiversity and Conservation 13: 1519-1539. - doi: 10.1023/B:BIOC.0000021326.50170.66
Dittus WPJ (2017). The biogeography and ecology of Sri Lankan mammals point to conservation priorities. Ceylon Journal of Science 46: 33-64. - doi: 10.4038/cjs.v46i5.7453
Dorado-Roda I, Pascual A, Godinho S, Silva C, Botequim B, Rodríguez-Gonzálvez P, González-Ferreiro E, Guerra-Hernández J (2021). Assessing the accuracy of GEDI data for canopy height and aboveground biomass estimates in Mediterranean forests. Remote Sensing 13 (12): 2279. - doi: 10.3390/rs13122279
Dubayah R, Blair JB, Goetz S, Fatoyinbo L, Hansen M, Healey S, Hofton M, Hurtt G, Kellner J, Luthcke S, Armston J, Tang H, Duncanson L, Hancock S, Jantz P, Marselis S, Patterson PL, Qi W, Silva C (2020). The global ecosystem dynamics investigation: high-resolution laser ranging of the Earth's forests and topography. Science of Remote Sensing 1: 100002. - doi: 10.1016/j.srs.2020.100002
Ediriweera S, Singhakumara BMP, Ashton MS (2008). Variation in canopy structure, light and soil nutrition across elevation of a Sri Lankan tropical rain forest. Forest Ecology and Management 256 (6): 1339-1349. - doi: 10.1016/j.foreco.2008.06.035
Egbert SL, Park S, Price KP, Lee R-Y, Wu J, Duane Nellis M (2002). Using conservation reserve program maps derived from satellite imagery to characterize landscape structure. Computers and Electronics in Agriculture 37 (1-3): 141-156. - doi: 10.1016/S0168-1699(02)00114-X
Gil A, Yu Q, Lobo A, Lourenço P, Silva L, Calado H (2011). Assessing the effectiveness of high resolution satellite imagery for vegetation mapping in small islands protected areas. Journal of Coastal Research 64: 1663-1667. [online] URL: http://www.jstor.org/stable/26482458
Grebner DL, Bettinger P, Siry JP (2013). Forest Measurements and Forestry-Related Data. In: "Introduction to Forestry and Natural Resources". Academic Press, S. Diego, USA, pp. 191-219. - doi: 10.1016/B978-0-12-386901-2.00008-7
Gunatilleke CVS, Gunatilleke IAUN (1985). Phytosociology of Sinharaja - A contribution to rain forest conservation in Sri Lanka. Biological Conservation 31 (1): 21-40. - doi: 10.1016/0006-3207(85)90032-1
Gunatilleke IAUN, Gunatilleke CVS, Dilhan MAAB (2005). Plant biogeography and conservation of the southwestern hill forests of Sri Lanka. The Raffles Bulletin of Zoology 12 (1): 9-22.
Gunatilleke N, Pethiyagoda R, Gunatilleke S (2008). Biodiversity of Sri Lanka. Journal of the National Science Foundation of Sri Lanka 36: 25-62. - doi: 10.4038/jnsfsr.v36i0.8047
Hancock S, Armston J, Hofton M, Sun X, Tang H, Duncanson LI, Kellner JR, Dubayah R (2019). The GEDI simulator: a large footprint waveform lidar simulator for calibration and validation of spaceborne missions. Earth and Space Science 6 (2): 294-310. - doi: 10.1029/2018EA000506
Hansen MC, Potapov PV, Moore R, Hancher M, Turubanova SA, Tyukavina A, Thau D, Stehman SV, Goetz SJ, Loveland TR, Kommareddy A, Egorov A, Chini L, Justice CO, Townshend JRG (2013). High-resolution global maps of 21st-century forest cover change. Science 342: 850-853. - doi: 10.1126/science.1244693
Han N, Wang K, Yu L, Zhang X (2012). Integration of texture and landscape features into object-based classification for delineating *Torreya* using IKONOS imagery. International Journal of Remote Sensing 33 (7): 2003-2033. - doi: 10.1080/01431161.2011.605084
Jayasekara D, Kumara PKPMP, Mahaulpatha WAD (2021). Mapping the vegetation cover and habitat categorization of Maduru Oya and Horton Plains National Parks using Landsat 8 (OLI) imagery to assist the ecological studies. Wildlanka 9 (1): 93-106. [online] URL: http://dr.lib.sjp.ac.lk/handle/123456789/10188
Kathriarachchi H (2012). Present status of lowland wet zone flora of Sri Lanka. In: "The National Red List 2012 of Sri Lanka" (Weerakoon DK, Wijesundara S eds). Biodiversity Secretariat of the Ministry of Environment and National Herbarium, Ministry of Environment, Colombo, Sri Lanka, pp. 175-452.
Li N, Lu D, Wu M, Zhang Y, Lu L (2018). Coastal wetland classification with multiseasonal high-spatial resolution satellite imagery. International Journal of Remote Sensing 39 (23): 8963-8983. - doi: 10.1080/01431161.2018.1500731
Li W, Dong R, Fu H, Wang J, Yu L, Gong P (2020). Integrating Google Earth imagery with Landsat data to improve 30-m resolution land cover mapping. Remote Sensing of Environment 237: 111563. - doi: 10.1016/j.rse.2019.111563
Lockwood I (2019). Preliminary analysis of land cover in the Sinharaja Adiviya using Planet Dove Imagery. Website. [online] URL: http://ianlockwood.blog/2019/09/16/preliminary-analysis-of-land-cover-in-the-sinharaja-adiviya-using-planet-dove-imagery/
Madhumali RMC, Wahala WMPSB, Sanjeewani HKN, Samarasinghe DP, De Costa WAJM (2021). Response of canopy leaf area index and architecture of tropical rainforests in Sri Lanka to climatic variation along an altitudinal gradient. Tropical Agricultural Research 32 (1): 1-16. - doi: 10.4038/tar.v32i1.8437
Madurapperuma B, Kuruppuarachchi J (2014). Change detection using mappable vegetation related indices - A case study from Sinharaja Forest Reserve. In: Proceedings of the "18th International Forestry and Environment Symposium. Department of Forestry and Environmental Science 2013". University of Sri Jayewardenepura, Nugegoda, Sri Lanka, pp. 69. - doi: 10.31357/fesympo.v18i0.1921
Marselis SM, Tang H, Armston J, Abernethy K, Alonso A, Barbier N, Bissiengou P, Jeffery K, Kenfack D, Labrière N, Lee S-K, Lewis SL, Memiaghe H, Poulsen JR, White L, Dubayah R (2019). Exploring the relation between remotely sensed vertical canopy structure and tree species diversity in Gabon. Environmental Research Letters 14: 094013. - doi: 10.1088/1748-9326/ab2dcd
Ma S, Zhou Y, Gowda PH, Dong J, Zhang G, Kakani VG, Wagle P, Chen L, Flynn KC, Jiang W (2019). Application of the water-related spectral reflectance indices: a review. Ecological Indicators 98: 68-79. - doi: 10.1016/j.ecolind.2018.10.049
Mtibaa S, Irie M (2016). Land cover mapping in cropland dominated area using information on vegetation phenology and multi-seasonal Landsat 8 images. Euro-Mediterranean Journal for Environmental Integration 1: 6. - doi: 10.1007/s41207-016-0006-5
Nissanka S, Pathinayake P (2009). Estimation of above-ground carbon stock in the Sinharaja Forest in Sri Lanka. In: Proceedings of the "First National Conference on Global Climate Change and its Impacts on Agriculture, Forestry and Water in the Tropics" (Nissanka S, Sangakkara UR eds). University of Peradeniya, Peradeniya, Sri Lanka, pp. 140-151.
Pantazi XE, Moshou D, Bochtis D (2020). Utilization of multisensors and data fusion in precision agriculture. In: "Intelligent Data Mining and Fusion Systems in Agriculture". (Pantazi XE, Moshou D, Bochtis D eds). Academic Press, S. Diego, USA, pp. 103-173. - doi: 10.1016/B978-0-12-814391-9.00003-0
Potapov P, Li X, Hernandez-Serna A, Tyukavina A, Hansen MC, Kommareddy A, Pickens A, Turubanova S, Tang H, Silva CE, Armston J, Dubayah R, Blair JB, Hofton M (2021). Mapping global forest canopy height through integration of GEDI and Landsat data. Remote Sensing of Environment 253: 112165. - doi: 10.1016/j.rse.2020.112165
Punchi-Manage R, Getzin S, Wiegand T, Kana-

garaj R, Savitri Gunatilleke CV, Nimal Gunatilleke IAU, Wiegand K, Huth A (2013). Effects of topography on structuring local species assemblages in a Sri Lankan mixed dipterocarp forest. Journal of Ecology 101 (1): 149-160. - doi: 10.1111/1365-2745.12017

R Core Team (2024). R: a language and environment for statistical computing. R Foundation for Statistical Computing, Vienna, Austria. [online] URL: http://www.R-project.org/

Samarasinghe JT, Gunathilake MB, Makubura RK, Arachchi SMA, Rathnayake U (2022). Impact of climate change and variability on spatiotemporal variation of forest cover in the World Heritage Sinharaja Rainforest, Sri Lanka. Forest and Society 6 (1): 355-377. - doi: 10.24259/fs.v6i1.18271

Schneider FD, Ferraz A, Hancock S, Duncanson LI, Dubayah RO, Pavlick RP, Schimel DS (2020). Towards mapping the diversity of canopy structure from space with GEDI. Environmental Research Letters 15 (11): 115006. - doi: 10.1088/1748-9326/ab9e99

Silva CA, Hamamura C, Valbuena R, Hancock S, Cardil A, Broadbent EN, Almeida DRA, Silva Junior CHL, Klauberg C (2023). rGEDI: NASA's Global Ecosystem Dynamics Investigation (GEDI) data visualization and processing, version 0.1.9. [online] URL: http://cran.r-project.org/package=rGEDI

Sykas D (2020). Spectral Indices with multispectral satellite data. Website. [online] URL: http://www.geo.university/pages/blog?p=spectral-indices-with-multispectral-satellite-data

Tierney DA, Powell T, Eriksson CE (2017). Vegetation mapping. Oxford Bibliographies in Ecology, website. [online] URL: http://www.oxfordbibliographies.com/display/document/obo-9780199830060/obo-9780199830060-0176.xml

Wang C, Elmore AJ, Numata I, Cochrane MA, Lei S, Hakkenberg CR, Li Y, Zhao Y, Tian Y (2022). A framework for improving wall-to-wall canopy height mapping by integrating GEDI LiDAR. Remote Sensing 14 (15): 3618. - doi: 10.3390/rs14153618

Wijesinghe MR, De Brooke L M (2005). Impact of habitat disturbance on the distribution of endemic species of small mammals and birds in a tropical rain forest in Sri Lanka. Journal of Tropical Ecology 21 (6): 661-668. - doi: 10.1017/S0266467405002695

Xie Y, Sha Z, Yu M (2008). Remote sensing imagery in vegetation mapping: a review. Journal of Plant Ecology 1 (1): 9-23. - doi: 10.1093/jpe/rtm005

Xie Z, Chen Y, Lu D, Li G, Chen E (2019). Classification of land cover, forest, and tree species classes with Ziyuan-3 multispectral and stereo data. Remote Sensing 11 (2): 164. - doi: 10.3390/rs11020164

Zurqani HA, Post CJ, Mikhailova EA, Schlautman MA, Sharp JL (2018). Geospatial analysis of land use change in the Savannah River Basin using Google Earth Engine. International Journal of Applied Earth Observation and Geoinformation 69: 175-185. - doi: 10.1016/j.jag.2017.12.006

Supplementary Material

Fig. S1 - Spatial distribution of the GEDI footprints.

Fig. S2 - Spatial variation of (a) elevation, (b) NDVI, (c) PAI, (d) PAVD, (e) CHM95 and (f) vegetation distribution of SFR.

Fig. S3 - Violin plot of PAI at different canopy strata of major vegetation types.

Fig. S4 - Variation of PAVD at different forest strata (a) 10m, (b) 20m, (c) 30m, (d) 45m and (e) total cumulative at 45m against canopy height.

Link: Jayasekara_4632@suppl001.pdf